arXiv:1701.07268v1 [physics.plasm-ph] 25 Jan 2017

Brilliant XUV radiation from laser-illuminated near-critical plasmas

T. G. Blackburn,[1,*] A. A. Gonoskov,[1,2,3] and M. Marklund[1]

[1] *Department of Physics, Chalmers University of Technology, SE-41296 Gothenburg, Sweden*
[2] *Institute of Applied Physics, Russian Academy of Sciences, Nizhny Novgorod 603950, Russia*
[3] *Lobachevsky State University of Nizhni Novgorod, Nizhny Novgorod 603950, Russia*

(Dated: January 26, 2017)

Bursts of extreme ultraviolet (XUV) radiation are generated by the nanoscale oscillations of surface electrons in plasmas illuminated by intense, linearly-polarised laser light. We show that this re-emission is especially efficient when the plasma electron density is between 1 and 10 times the relativistic critical density and the laser incidence angle is 60°. The resulting XUV flash, averaged over the reflected pulse duration, has brilliance in excess of 10^{23} photons/s/mm^2/mrad^2 (0.1% bandwidth) in the 10–100 eV range, far above that of a third-generation synchrotron light source.

I. INTRODUCTION

There has been extensive demonstration of radiation sources in the extreme ultraviolet (XUV) to X-ray frequency range employing laser illumination of solid [1–5] and gaseous targets [6–8]. High-frequency radiation naturally arises in these interactions due to the nonlinear motion of electrons oscillating in the strong electromagnetic fields of a relativistically intense laser pulse. The generation efficiency and spectral properties of XUV sources are of paramount importance for applications in diagnostic imaging [9, 10], the creation and study of warm dense matter [11, 12] and for probing attosecond phenomena [13].

Here we show that illuminating plasmas with electron density between 1 and 10 times the relativistic critical density at 60° under realistic conditions couples >3% of the laser energy to harmonics with energy $\omega > 10$ eV. The brilliance of the reflected light, 10^{23} photons s^{-1} mm^{-2} mrad^{-2} at 0.1% bandwidth at 100 eV, is unprecedented in laser-solid interactions and realisable at currently available high-intensity, short-pulse laser facilities. The physical origin of this radiation is near-micron scale oscillation of the plasma surface, which temporarily stores a large fraction of the laser energy in a longitudinal electric field; this compresses the re-emission into an attosecond burst that has larger amplitude than the incident light [14, 15].

We use three dimensionless parameters to characterise the laser-plasma interaction: $a_0 = eE/(mc\omega)$, the normalised amplitude of an electromagnetic wave with electric field strength E and angular frequency ω; θ, the angle between the laser wavevector and the target normal; and S, the ratio of the electron number density n_e to that of the relativistic critical density $a_0 n_{\rm cr}$ [16]. Here $n_{\rm cr} = \epsilon_0 m\omega^2/e^2$ is the non-relativistic critical density, and e, m are the electron charge and mass, c the speed of light, with ϵ_0 the vacuum permittivity. A convenient approximation accurate within 5% is

$$S = \frac{n_e}{a_0 n_{\rm cr}} \simeq \frac{n_{23}\lambda_{\mu\rm m}}{\sqrt{I_{22}}} \tag{1}$$

where n_{23} is the electron number density in units of 10^{23} cm^{-3}, I_{22} is the laser intensity in units of 10^{22} Wcm^{-2} and $\lambda_{\mu\rm m}$ its wavelength in microns.

An overdense plasma, through which light cannot propagate, is typically characterised by $S \gtrsim 1$. In this regime laser energy must be either reflected or absorbed by electron heating and ion motion. For highly-overdense targets ($S \gg 1$) electron heating is minimal and most of the laser energy is reflected. At moderate intensities, coherent wake emission leads to harmonic generation in the ultraviolet [3]; at higher intensities, experiments have demonstrated conversion efficiencies of 0.01 (10^{-5}) to X-rays with energy greater than 20 eV (1 keV) [17], or 10^{-4} in the tens of eV at $a_0 \simeq 3$ [18].

Harmonic generation in the regime $S \gg 1$ can be described under the assumption that the overdense surface acts as a *relativistic oscillating mirror* (ROM), perfectly reflecting the incident light at every instant of time within the wave cycle from a certain oscillating point [19, 20]. The Doppler shift when this point moves back towards the the observer at relativistic velocity leads to the increase in frequency of the reflected light. Models based on this assumption have given insight into polarisation selection rules [20, 21], the angular dependence of generation efficiency [22], and the power-law form of the intensity spectrum [23–27].

We consider here plasmas with electron density $S < 10$ (but above the threshold for relativistic self-induced transparency), where the reflection process is not instantaneous. Instead energy is first accumulated in a charge separation field when the laser radiation pressure displaces electrons from the plasma-vacuum boundary. This energy is then re-emitted when the electrons propagate back towards the boundary. Due to the relativistic nature of the motion, the displaced electrons are compressed into a thin layer. The *relativistic electron spring* (RES) model of Gonoskov *et al.* [14] successfully describes these interactions by assuming that emission from the separated ions and electrons compensates the incident radia-

* tom.blackburn@chalmers.se

tion within the plasma bulk, while allowing energy accumulation in the separation region.

Emission of a thin layer has been studied in the context of creating reflected and transmitted attosecond pulses [28, 29] and in thin-foil interactions [30, 31]. Such a layer forms automatically in the RES regime leading to the emission of attosecond [32] bursts with amplitude several times that of the incident light [14, 15, 33], as well as bright incoherent beams [34].

If the reflected amplitude exceeds the incident amplitude by a factor $f \gg 1$ for $S < 10$, and with the assumption that the plasma is perfectly reflective, an amplitude increase of f implies that the temporal width of the pulse is reduced by a factor f^2 and so characteristic harmonics are produced of order $n \simeq f^2$. It is therefore advantageous to access the RES regime of plasma dynamics to ensure efficient generation of high harmonics.

There has been considerable work devoted to optimising XUV generation [35], including PIC simulation of few-cycle lasers [29, 36], development of analytics [14, 22] and experiment. It has been shown, for example, that the denting of the plasma surface by the laser light pressure, which would otherwise increase the divergence of the high harmonics, may be compensated by tailoring the input laser pulse [37]. Simulations have also demonstrated the advantages of multiple reflection geometries [38] and specially-designed waveforms for the incident light [39]. Here we focus on the basic properties of the laser-plasma interaction with a view to optimising the XUV yield.

The paper is laid out as follows: first, we show in detail the advantages of the RES mechanism by comparing the illumination of a near-critical and a highly-overdense plasma in section II. Then in section III we use 1D particle-in-cell (PIC) simulations to find the laser-target configuration that maximises XUV generation. Having shown that this is a plasma with $S \simeq 1$ illuminated by laser light at an angle of $\theta = 60°$, much as RES theory predicts, we turn to 2D PIC simulation results in section IV. We present our results for the angular and brilliance properties of the XUV pulse and show that the 1D and 2D results are broadly consistent. We conclude by discussing the prospects of our work in section V.

II. THE RELATIVISTIC ELECTRON SPRING MECHANISM

The interaction geometry under consideration is shown in fig. 1a: we have a laser pulse with normalised amplitude a_0 and angular frequency ω incident on a cold plasma with electron density $Sa_0 n_{\rm cr}$ at an angle θ to the target normal. We will assume that the ions are sufficiently massive that they do not move. For the moment we work in the frame boosted by $c\sin\theta$ in the direction parallel to the plasma surface. Neglecting the transverse intensity variation of a focussed laser pulse, in this frame the laser may be treated as a plane wave with amplitude $a_0\cos\theta$ normally incident on a plasma with density

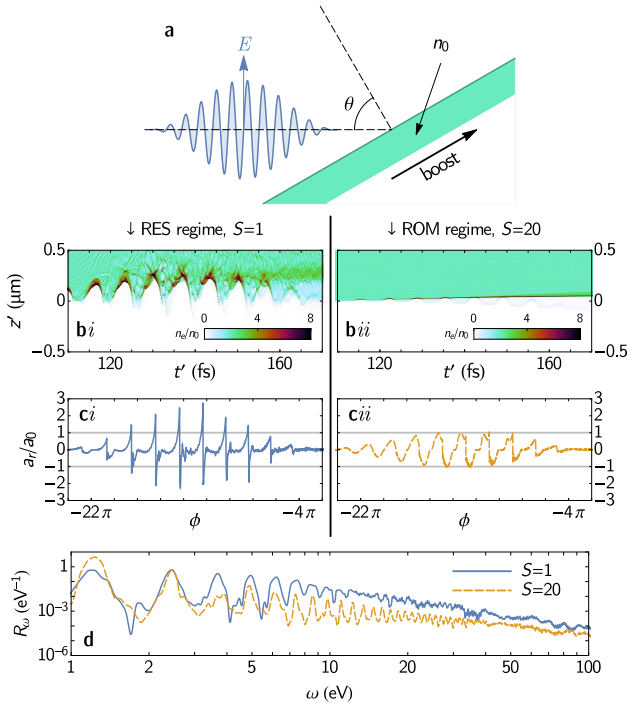

FIG. 1. a) The interaction geometry under consideration is a p-polarised laser pulse incident on a semi-infinite plasma slab with initial electron density $n_0 = Sa_0 n_{\rm cr}$ at an angle to the target normal of θ. b) The electron density n_e/n_0 in the boosted frame (see text) as a function of axial displacement z' and time t' when laser light with peak amplitude $a_0 = 60.4$ is incident at 60° onto plasma with (i) $S = 1$ and (ii) $S = 20$. c) In the lab frame, the amplitude of the reflected light a_r relative to the initial amplitude a_0 for (i, blue) $S = 1$ and (ii, yellow-dashed) $S = 20$. d) The reflectivity per unit frequency R_ω of the plasma, i.e. Fourier spectra of the pulses shown in c).

$n_0/\cos\theta$ and streaming velocity $c\sin\theta$ perpendicular to the target normal. Therefore the problem is reduced to one with a single spatial dimension [40].

To demonstrate the advantages of the RES mechanism, we compare the results of 1D3V particle-in-cell (PIC) simulations using the spectral code ELMIS [41] of plasma with $S = 1$ and $S = 20$. The former is within the RES regime; the latter in the ROM regime. In both cases the laser has lab-frame profile $a_0 \sin\phi\cos^2(\phi/24)$ with $a_0 = 60.4$ and wavelength $\lambda = 1\,\mu$m; this corresponds to a peak intensity of $5\times10^{21}\,{\rm Wcm}^{-2}$ and full width at half maximum (FWHM) of 15 fs. In the boosted frame, the laser has phase $\phi = \omega\cos\theta(t' - z'/c)$ and is p-polarised (along x'). The plasma is initialised with density profile $n_{e,0} = Sa_0 n_{\rm cr} H(z')/\cos\theta$, where H is the Heaviside step function, velocity $v_{x',0}/c = -\sin\theta$ and temperature 100 eV. It is represented by 200 (macro-)electrons and ions ($Z/A = 0.05$) per cell of size $\Delta z' = \lambda/(1800\cos\theta)$.

Figure 1b shows the electron density as a function of axial displacement z' and time t'. The oscillations arise

because the laser radiation pressure pushes electrons into the plasma, gathering them into a thin region of high charge density at z'_e. The uncompensated ion current in the region $0 < z' < z'_e$ sets up electrostatic and magnetostatic fields, the former exerting a force on the electron density spike that balances and then exceeds the radiation pressure. The fact that this force is proportional to the displacement z'_e, assuming the downstream region is entirely cleared of electrons, is the origin of the name 'relativistic electron spring' [14].

During the phase of the motion when the electrons return towards $z' = 0$, they acquire kinetic energy from the plasma fields, reaching high γ. When their transverse velocity changes sign, at which moment in the lab frame they propagate towards the observer along the specular direction, a large-amplitude burst of radiation is emitted. This is shown in fig. 1c: for $S = 20$, the waveform acquires a non-sinusoidal shape but the amplitude does not exceeed a_0, whereas for $S = 1$ for the waveform is characterised by sharp transitions between positive and negative field and amplitude increase $f = \max(a_r/a_0) \simeq 3$. The consequence of this is seen in the Fourier analysis of the reflected intensity R_ω shown in fig. 1d: the high-harmonic intensity is an order of magnitude larger for $S = 1$ across the spectral range $\omega > 10$ eV.

This is broadly consistent with theoretical predictions: RES theory predicts a frequency spectrum that decays quasi-exponentially with harmonic order [14], in contrast to the power-law decay $\partial I/\partial\omega \propto \omega^{-m}$ expected in the ROM regime. Baeva *et al.* [23] predict a universal $m = 8/3$, but a range $5/3 < m < 7/3$ is seen in PIC simulation [26]; in any case, weakening of the power-law decay to $m \simeq 1.62$ has been observed in thin-foil experiments where XUV emission may attributed to electron nanobunches [28].

However, in these results the two processes are partially mixed due to the effect of the laser temporal profile. The effective S varies across the pulse: the leading edge encountering a clean, sharp transition to $S > 1$, whereas the trailing edge encounters a surface with finite density gradient. This is why the difference between RES and ROM shown in fig. 1c is clearest in the leading edge of the reflected pulse (towards negative ϕ). For the case $S = 20$, a pre-plasma of lower density is pulled out into vacuum as the surface breaks up under the action of the intense pulse; the trailing edge of the incident light reflects from this lower density region, leading to the RES-like features seen towards positive ϕ in fig. 1c.

A full analysis of the effect of pre-plasma and its relation to the laser pulse length is beyond the scope of this work; it suffices here to indicate that where we refer to the optimal S of a clean plasma interaction, our results will apply to laser pulses reflecting from long scale-length pre-plasma before highly overdense targets.

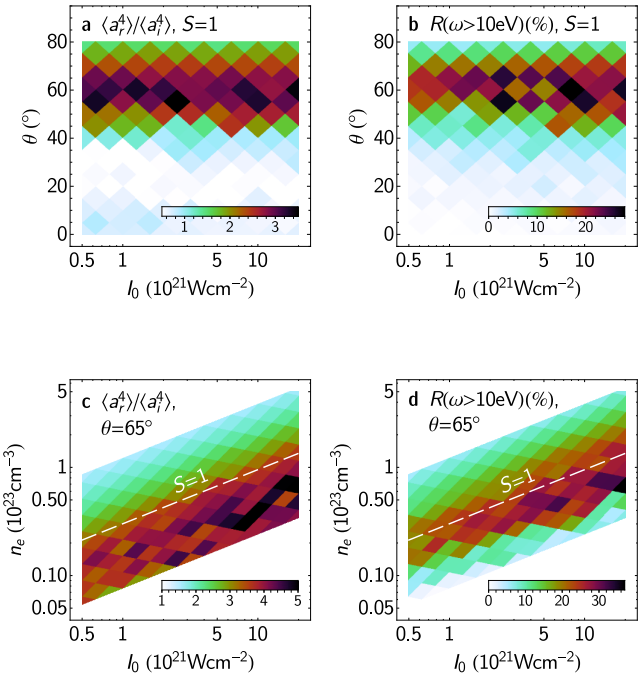

FIG. 2. The increase in the peak amplitude (a,c) and the percentage of laser energy converted to XUV with $\omega > 10$ eV (b,d) when plasma with electron density $n_e = Sa_0 n_{\rm cr}$ is illuminated by laser light with peak intensity I_0 at an angle θ to the target normal. In (a,b) S is fixed at $S = 1$ and the intensity and angle of incidence are varied; in (c,d), the angle of incidence is fixed at $\theta = 65°$ and the intensity and density varied. Intensities and densities for which $S = 1$ are indicated with dashed lines.

III. OPTIMAL DENSITY AND ANGLE OF INCIDENCE

We now discuss how the plasma density and angle of incidence can be chosen to maximise the increase in reflected amplitude and the yield of high harmonics. Previous work considering single-wavelength light indicates that an optimum exists for plasma with $S \simeq 0.5$ and $\theta \simeq 62°$ [14]. To check this, we have performed a parameter scan in laser intensity I_0, plasma density n_e and angle of incidence θ with 1D PIC simulation. The laser pulse shape and other simulation parameters are as used in fig. 1. The covered range is $5 \times 10^{20}\,\mathrm{Wcm}^{-2} \leq I_0 \leq 10^{22}\,\mathrm{Wcm}^{-2}$, $1/4 \leq S \leq 4$, and $0° < \theta < 80°$.

The figures of merit we use to characterise the interaction are the 4$^{\rm th}$ order average amplitude and the XUV reflectivity. We define the $n^{\rm th}$ order average amplitude $\langle a_r^n\rangle / \langle a_i^n\rangle \equiv \int a_r^n \,\mathrm{d}V / \int a_i^n \,\mathrm{d}V$, where the integral is calculated over the entire spatial domain of the pulse, for incident and reflected waveforms $a_{i,r}$ and even integer n. Setting $n = 2$ would be equivalent to calculating the reflectivity of the plasma, so $0 \leq \langle a_r^2\rangle / \langle a_i^2\rangle \leq 1$ for all I_0, n_e and θ. By setting $n = 4$ instead, we en-

hance the contribution of large-amplitude components to the integral and therefore acquire a measure of the amplitude increase. The XUV conversion efficiency R is calculated by transforming the backward-propagating electric and magnetic fields to the lab frame and performing Fourier analysis to determine the reflectivity per unit frequency $R_\omega \equiv (\partial U_r/\partial\omega)/U_i$, where $U_{i,r}$ is the energy of the incoming and outgoing pulses respectively. Then $R \equiv \int_{\omega_{\min}} R_\omega \mathrm{d}\omega$ for some minimal energy $\omega_{\min}$, which we set to 10 eV. For the waveforms shown in fig. 1c, where $I_0 = 5\times10^{21}\,\mathrm{Wcm}^{-2}$ and $\theta = 60°$, we have that: $\langle a_r^4\rangle / \langle a_i^4\rangle = 2.1$ and $R = 0.24$ for $S = 1$; and $\langle a_r^4\rangle / \langle a_i^4\rangle = 1.0$ and $R = 0.030$ for $S = 20$.

Let us first consider the situation where S is fixed to be 1 and the intensity and angle of incidence are varied, shown in figs. 2a and 2b. Here the electron density n_e is implicitly increased with intensity as required by eq. (1). There is a broad maximum in $\langle a_r^4\rangle / \langle a_i^4\rangle$ between 45° and 75°, over which interval the peak intensity of the reflected pulse is increased by almost a factor of 10. Associated with this is a strong increase in the conversion efficiency to >10 eV light: there is little XUV emission for $\theta \lesssim 20°$ but more than 20% of the pulse is converted for $55° \gtrsim \theta \lesssim 75°$. Furthermore, neither the amplitude increase nor conversion efficiency demonstrate a strong dependence on intensity, which is consistent with the S-scaling of plasma dynamics proposed by Gordienko and Pukhov [16]. The optimal angle $\theta \simeq 60°$ is consistent with that proposed in Gonoskov *et al.* [14].

Fixing the angle of incidence at 65°, we explore intensity-density space in figs. 2c and 2d. These results are also consistent with the S-scaling: provided the density is matched to the intensity as specified by eq. (1), the amplitude increase and XUV reflectivity are constant at the 10% level even though the intensity increases by a factor of 40. Figure 2d shows that there is broad maximum in the XUV reflectivity for plasma with $0.5 \lesssim S \lesssim 2$. This threshold is consistent with theoretical expectations Gonoskov *et al.* [14]. The fact that $S = 0.5$ is a threshold rather than a maximum is an effect of laser temporal envelope: if the density is set so that $S = 0.5$ is achieved at the pulse centre, there is sufficient electron heating that the sharp surface breaks up under the action of the pulse foot.

Figure 2c shows that the increase in the reflected amplitude is maximised for slightly lower S than the XUV reflectivity, which is not consistent with our simple expectation that the two should be maximised together. The origin of this is a change in the character of the reflected waveform when moving to lower density. The number of attosecond bursts is set by the number of times the electron nanobunch's transverse velocity $\beta_{x'}$ (in the boosted frame) changes sign. In the optimal regime, this occurs once per laser period, leading to a concentration of the reflected energy in a single emission event. As the velocity changes sign, so too does the sign of the reflected amplitude, leading to the sharp transitions between positive and negative field shown in fig. 1c. However, if $S \lesssim 0.25$, it occurs that the nanobunch velocity merely grazes the $\beta_{x'} = 0$ axis, and the reflected waveform is unipolar rather than bipolar, with longer duration. This reduces the XUV reflectivity even though the amplitude is still increased across the range $0.25 \leq S < 2$.

We may conclude that for a laser pulse with realistic temporal profile, irradiating plasma with $0.5 \leq S < 2$ at $50° \leq \theta \leq 70°$ leads to conversion of 30% of the incident energy to harmonics with energy $\omega > 10\,\mathrm{eV}$, with an associated increase in the peak intensity. Furthermore, the agreement between the 1D theory of Gonoskov *et al.* [14] and simulation for a realistic pulse shape is excellent.

IV. PROPERTIES OF THE XUV PULSE

In this spirit, we have carried out a parameter scan in S and θ with the 2D3V PIC code EPOCH [42]. For all simulations, the laser is focussed to a spot with waist $4\,\mu$m at the plasma surface and peak intensity $5\times10^{21}\,\mathrm{Wcm}^{-2}$ ($a_0 = 60.4$). Its temporal profile and wavelength are the same as in the 1D simulations: $\sin^2$ with FWHM 15 fs and $\lambda = 1\,\mu$m respectively. The simulation domain, $[0,16]\times[-3,24]\lambda$ in the x and y-directions, contains electron-ion plasma ($Z/A = 0.05$) in the region $y \leq 0$. The resolution varies between 200 and 500 cells per λ, and the number of particles per cell between 24 and 48 for each species. The laser is injected from the left boundary at an angle θ to the target normal; to reduce the length of plasma, and so the number of computational particles, required to model the interaction, the simulation domain moves along x with velocity $c\sin\theta$. The amplitude and harmonic content of the reflected light is analysed once the pulse has moved a perpendicular distance of $12\,\mu$m from the plasma surface. The explored range is $0.5 \leq S < 15$ and $30° \leq \theta \leq 70°$.

In moving from one to two spatial dimensions we encounter two new physical effects that alter the XUV generation process. The first is that the conservation of transverse kinetic momentum, which applies exactly in 1D, is lifted, leading to increased electron heating and reduction of the plasma reflectivity. Secondly, the variation in laser intensity across the plasma surface (or, equivalently, the variation in the effective S) leads to a spatially varying displacement of the electron-ion boundary and to wavefront curvature of the reflected light. Both of these effects are more pronounced for plasma of lower S.

In figs. 3a to 3c we show snapshots of the amplitude of the reflected light for incidence angle 60° and S of 0.5, 4 and 8. For the lowest density, we see that the wavefronts of the leading edge are almost flat, corresponding to reflection in the specular direction. The lineout along this vector shows the sharp spikes that are characteristic of the RES mechanism. Towards the peak of the pulse, where the amplitude reaches near twice its initial value, the wavefronts are become curved due to ponderomotive denting of the plasma surface. Behind this, however, the RES spikes are lost as the laser reflects from that non-

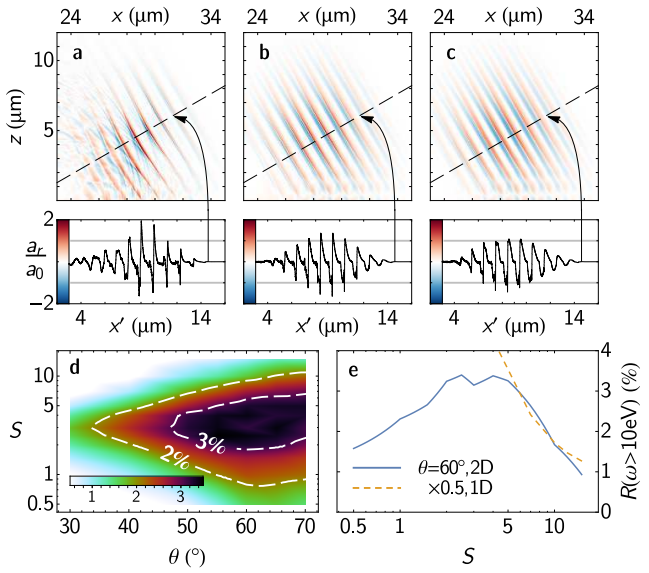

FIG. 3. (a-c) (upper) Colour maps and (lower) lineouts along the specular direction of the amplitude of light reflected from a plasma with $S =$ a) 0.5, b) 4 and c) 8 illuminated by a laser pulse with peak intensity $5 \times 10^{21}\,\mathrm{Wcm}^{-2}$ at an incidence angle $\theta = 60°$. d) The percentage of laser energy converted to radiation with $10\,\mathrm{eV} < \omega < 50\,\mathrm{eV}$ and e) comparing a (blue, solid) lineout of that conversion efficiency along $\theta = 60°$ to (yellow, dashed) that predicted by 1D simulations, scaled by 0.5.

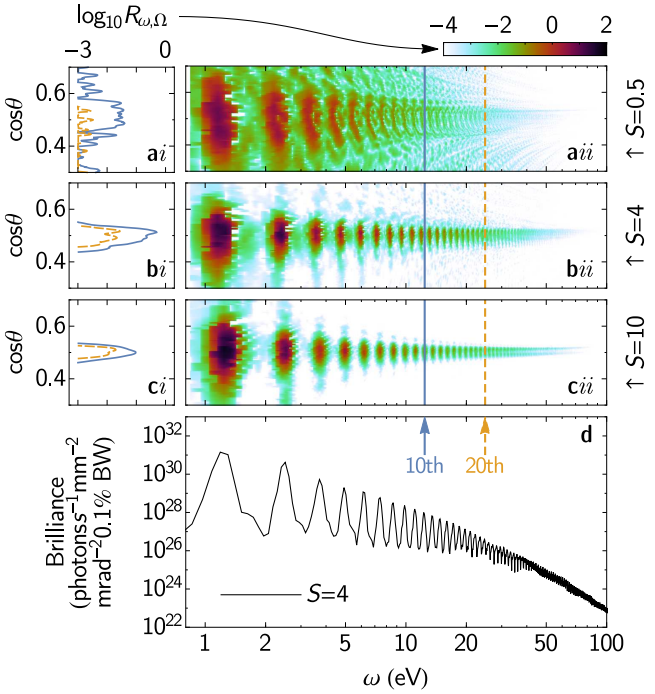

FIG. 4. (a–c) $R_{\omega,\Omega}$, the reflectivity per unit photon energy ω per unit solid angle $\cos\theta$, for plasma with $S =$ a) 0.5, b) 4, and c) 10 illuminated by a laser pulse with peak intensity $5 \times 10^{21}\,\mathrm{Wcm}^{-2}$, wavelength $1\,\mu$m and waist $4\,\mu$m, showing slices through colour maps *ii*) at the (blue, solid) 10th and (yellow, dashed) 20th harmonics. (d) The brilliance for $S = 4$.

uniform plasma surface.

These effects are mitigated by moving to higher S. For $S = 4$, fig. 3b shows that the wavefronts are near flat across the entire pulse. While the amplitude is only increased to 1.2× its initial value, RES-like features can be seen across the whole of the reflected waveform. Similarly to fig. 2c, fig. 3c shows that at $S = 8$, the leading edge of the pulse acquires the non-linear reshaping characteristic of the ROM mechanism.

The consequence of increased electron heating and non-uniformity of the plasma surface is to shift the optimum for XUV generation from $S = 1$ to $S \simeq 4$. Nevertheless, the XUV reflectivity shown in fig. 3d still has the broad peak between 50° and 70° we expect based on 1D theory and simulation, and fig. 3e shows that for $S > 4$, the 2D reflectivity is within a factor of two that predicted by 1D simulations. Even though we expect losses to electron heating to become larger when irradiating near-critical plasmas, this is outweighed by the XUV reflectivity increase attributable to the storage of energy in plasma fields during non-linear motion of the plasma surface.

Furthermore, the emission of these harmonics is closely collimated along the specular direction, with angular divergence comparable to that of the incoming laser pulse. We show in fig. 4 colour maps of $R_{\omega,\Omega}$, the reflectivity per unit frequency ω and solid angle $\cos\theta$. The harmonics become more distinct, with smaller divergence, as S increases. Slices at the 10^{th} and 20^{th} harmonics show that for $S = 4$ and 10 the reflected energy is concentrated within a window $\Delta(\cos\theta) \simeq 0.05$, corresponding to a half-angle of 3° at 60°. For comparison, the incident laser pulse with waist $w_0 = 4\,\mu$m and wavelength $1\,\mu$m has half-angle divergence $\theta_{\mathrm{laser}} = \lambda/(\pi w_0) \simeq 5°$. One might expect that the wavelength dependence in this relation leads to decreasing divergence with increasing harmonic order. However fig. 4 shows that the divergence of the 20^{th} harmonic is near, not half, that of the 10^{th}, and therefore the dominant effect is the overall divergence of the laser pulse.

The distribution of energy in ω and $\cos\theta$ is broader and noisier for $S = 0.5$ than it is for $S = 4, 10$. The broadening is caused by ponderomotive denting of the plasma surface, which increases the curvature of the reflected wavefronts as shown in fig. 3a. Break-up of the plasma surface and ejection of hot electrons then leads to the emission of high-frequency radiation away from the specular axis. We note that despite these losses, the peak reflected intensity in this case is four times its initial value. For the initial conditions under consideration here, this corresponds achieving over two cycles a reflected intensity of $2 \times 10^{22}\,\mathrm{Wcm}^{-2}$, equal to the current record [43]. It has been proposed that curved plasma surfaces may

be used to focus high harmonics to extreme intensity, exploiting the reduction in the diffraction limit [44]; such effects would stand in addition to the intensity increase arising from the RES mechanism.

Finally, we use the spectral reflectivity from simulation to estimate the brilliance, which is a measure of photon phase-space density. Assuming a fiducial distance in the z-direction (perpendicular to the simulation plane) of 1 μm, a duration equal to the laser pulse FWHM of 15 fs, and a half-angle divergence of 3°, we show in fig. 4 that the brilliance is of order 10^{23} photons/s/mm^2/mrad^2 (0.1% bandwidth) at $\omega = 100\,\mathrm{eV}$, for the optimal parameters of $S = 4$, $\theta = 60°$. This is five orders of magnitude larger than that achieved in third-generation synchrotron light sources [45].

V. CONCLUSIONS

We have explored how the relativistic electron spring mechanism leads to bright bursts of XUV radiation when plasma with electron density n_e satisfying $1 < S = n_e/(a_0 n_{\mathrm{cr}}) < 10$ is illuminated by intense laser light ($a_0 \gg 1$). The physical origin of this enhanced emission is the storage of energy in plasma electromagnetic fields when the electron-ion boundary is displaced by the oscillating radiation pressure of the laser. We have justified the theoretical prediction of the optimal parameters $S = 1$, $\theta = 60°$ with high-resolution 1D PIC simulation, and shown with 2D simulations that for the near-critical plasmas required to probe this regime, increased electron heating is not sufficient to overcome the intrinsic advantage of the RES process. This can generate reflected EM radiation with peak intensity four times higher than the incident intensity even in planar geometry, as well as high harmonics collimated at the degree-level. The conversion efficiency of >3% leads to brilliances in the 10s of eV unprecedented in laser-solid interactions.

ACKNOWLEDGMENTS

The authors acknowledge support from the Knut and Alice Wallenberg Foundation (T.B., A.G., M.M.), the Swedish Research Council (grants 2012-5644 and 2013-4248, M.M.), the Russian Science Foundation (project no. 16-12-10486, A.G.) and the Russian Foundation for Basic Research (project no. 15-37-21015, A.G.). Simulations were performed on resources provided by the Swedish National Infrastructure for Computing (SNIC) at the High Performance Computing Centre North (HPC2N).

[1] A. Rousse, P. Audebert, J. P. Geindre, F. Falliès, J. C. Gauthier, A. Mysyrowicz, G. Grillon, and A. Antonetti, Phys. Rev. E **50**, 2200 (1994).
[2] B. Dromey, M. Zepf, A. Gopal, K. Lancaster, M. S. Wei, K. Krushelnick, M. Tatarakis, N. Vakakis, S. Moustaizis, R. Kodama, M. Tampo, C. Stoeckl, R. Clarke, H. Habara, D. Neely, S. Karsch, and P. Norreys, Nature Phys. **2**, 456 (2006).
[3] F. Quéré, C. Thaury, P. Monot, S. Dobosz, P. Martin, J.-P. Geindre, and P. Audebert, Phys. Rev. Lett. **96**, 125004 (2006).
[4] U. Teubner and P. Gibbon, Rev. Mod. Phys. **81**, 445 (2009).
[5] B. Dromey, D. Adams, R. Hörlein, Y. Nomura, S. G. Rykovanov, D. C. Carroll, P. S. Foster, S. Kar, K. Markey, P. McKenna, D. Neely, M. Geissler, G. D. Tsakiris, and M. Zepf, Nature Phys. **5**, 146 (2009).
[6] A. Rousse, K. T. Phuoc, R. Shah, A. Pukhov, E. Lefebvre, V. Malka, S. Kiselev, F. Burgy, J.-P. Rousseau, D. Umstadter, and D. Hulin, Phys. Rev. Lett. **93**, 135005 (2004).
[7] S. Kneip, C. McGuffey, J. L. Martins, S. F. Martins, C. Bellei, V. Chvykov, F. Dollar, R. Fonseca, C. Huntington, G. Kalintchenko, A. Maksimchuk, S. P. D. Mangles, T. Matsuoka, S. R. Nagel, C. A. J. Palmer, J. Schreiber, K. Ta Phuoc, A. G. R. Thomas, Y. V., L. O. Silva, K. Krushelnick, and Z. Najmudin, Nature Phys. **6**, 980 (2010).
[8] S. Corde, K. Ta Phuoc, G. Lambert, R. Fitour, V. Malka, A. Rousse, A. Beck, and E. Lefebvre, Rev. Mod. Phys. **85**, 1 (2013).
[9] S. Dobosz, G. Doumy, H. Stabile, P. D'Oliveira, P. Monot, F. Réau, S. Hüller, and P. Martin, Phys. Rev. Lett. **95**, 025001 (2005).
[10] C. M. Brenner, S. R. Mirfayzi, D. R. Rusby, C. Armstrong, A. Alejo, L. A. Wilson, R. Clarke, H. Ahmed, N. M. H. Butler, D. Haddock, A. Higginson, A. McClymont, C. Murphy, M. Notley, P. Oliver, R. Allott, C. Hernandez-Gomez, S. Kar, P. McKenna, and D. Neely, Plasma Phys. Control. Fusion **58**, 014039 (2016).
[11] B. Nagler *et al.*, Nature Phys. **5**, 693 (2009).
[12] E. Galtier, F. B. Rosmej, T. Dzelzainis, D. Riley, F. Y. Khattak, P. Heimann, R. W. Lee, A. J. Nelson, S. M. Vinko, T. Whitcher, J. S. Wark, T. Tschentscher, S. Toleikis, R. R. Fäustlin, R. Sobierajski, M. Jurek, L. Juha, J. Chalupsky, V. Hajkova, M. Kozlova, J. Krzywinski, and B. Nagler, Phys. Rev. Lett. **106**, 164801 (2011).
[13] F. Krausz and M. Ivanov, Rev. Mod. Phys. **81**, 163 (2009).
[14] A. A. Gonoskov, A. V. Korzhimanov, A. V. Kim, M. Marklund, and A. M. Sergeev, Phys. Rev. E **84**, 046403 (2011).
[15] D. an der Brügge and A. Pukhov, Phys. Plasmas **17**, 033110 (2010), 10.1063/1.3353050.
[16] S. Gordienko and A. Pukhov, Phys. Plasmas **12**, 043109 (2005), 10.1063/1.1884126.
[17] B. Dromey, S. Kar, C. Bellei, D. C. Carroll, R. J. Clarke, J. S. Green, S. Kneip, K. Markey, S. R. Nagel, P. T. Simpson, L. Willingale, P. McKenna, D. Neely, Z. Najmudin, K. Krushelnick, P. A. Norreys, and M. Zepf,

Phys. Rev. Lett. **99**, 085001 (2007).
[18] C. Rödel, D. an der Brügge, J. Bierbach, M. Yeung, T. Hahn, B. Dromey, S. Herzer, S. Fuchs, A. G. Pour, E. Eckner, M. Behmke, M. Cerchez, O. Jäckel, D. Hemmers, T. Toncian, M. C. Kaluza, A. Belyanin, G. Pretzler, O. Willi, A. Pukhov, M. Zepf, and G. G. Paulus, Phys. Rev. Lett. **109**, 125002 (2012).
[19] S. V. Bulanov, N. M. Naumova, and F. Pegoraro, Phys. Plasmas **1**, 745 (1994).
[20] R. Lichters, J. MeyerterVehn, and A. Pukhov, Phys. Plasmas **3**, 3425 (1996).
[21] D. von der Linde and K. Rzàzewski, Appl. Phys. B **63**, 499 (1996).
[22] A. Debayle, J. Sanz, and L. Gremillet, Phys. Rev. E **92**, 053108 (2015).
[23] T. Baeva, S. Gordienko, and A. Pukhov, Phys. Rev. E **74**, 046404 (2006).
[24] A. S. Pirozhkov, S. V. Bulanov, T. Z. Esirkepov, M. Mori, A. Sagisaka, and H. Daido, Phys. Plasmas **13**, 013107 (2006).
[25] A. Debayle, J. Sanz, L. Gremillet, and K. Mima, Phys. Plasmas **20**, 053107 (2013).
[26] T. J. M. Boyd and R. Ondarza-Rovira, Phys. Rev. Lett. **101**, 125004 (2008).
[27] T. J. M. Boyd and R. Ondarza-Rovira, Phys. Lett. A **380**, 1368 (2016).
[28] B. Dromey, S. Cousens, S. Rykovanov, Y. M., D. Jung, D. C. Gautier, T. Dzelzainis, D. Kiefer, S. Palaniyppan, R. Shah, J. Schreiber, J. C. Fernandez, C. L. S. Lewis, M. Zepf, and B. M. Hegelich, New Journal of Physics **15**, 015025 (2013).
[29] S. Cousens, B. Reville, B. Dromey, and M. Zepf, Phys. Rev. Lett. **116**, 083901 (2016).
[30] J. M. Mikhailova, M. V. Fedorov, N. Karpowicz, P. Gibbon, V. T. Platonenko, A. M. Zheltikov, and F. Krausz, Phys. Rev. Lett. **109**, 245005 (2012).
[31] S. V. Bulanov, T. Z. Esirkepov, M. Kando, S. S. Bulanov, S. G. Rykovanov, and F. Pegoraro, Phys. Plasmas **20** (2013), 10.1063/1.4848758.
[32] A. V. Bashinov, A. A. Gonoskov, A. V. Kim, G. Mourou, and A. M. Sergeev, Eur. Phys. J. Spec. Top. **223**, 1105 (2014).
[33] J. Fuchs, A. A. Gonoskov, M. Nakatsutsumi, W. Nazarov, F. Quéré, A. M. Sergeev, and X. Q. Yan, Eur. Phys. J. Spec. Top. **223**, 1169 (2014).
[34] D. A. Serebryakov, E. N. Nerush, and I. Y. Kostyukov, Phys. Plasmas **22** (2015), 10.1063/1.4938206.
[35] G. Sansone, L. Poletto, and N. Mauro, Nat. Photon. **5**, 655 (2011).
[36] G. D. Tsakiris, K. Eidmann, J. Meyer-ter-Vehn, and F. Krausz, New Journal of Physics **8**, 19 (2006).
[37] H. Vincenti, S. Monchocé, S. Kahaly, G. Bonnaud, P. Martin, and F. Quéré, Nat. Commun. **5** (2014), 10.1038/ncomms4403.
[38] M. R. Edwards and J. M. Mikhailova, Phys. Rev. A **93**, 023836 (2016).
[39] M. R. Edwards and J. M. Mikhailova, Phys. Rev. Lett. **117**, 125001 (2016).
[40] A. Bourdier, Phys. Fluids **26**, 1804 (1983).
[41] A. Gonoskov, S. Bastrakov, E. Efimenko, A. Ilderton, M. Marklund, I. Meyerov, A. Muraviev, A. Sergeev, I. Surmin, and E. Wallin, Phys. Rev. E **92**, 023305 (2015).
[42] T. D. Arber, K. Bennett, C. S. Brady, A. Lawrence-Douglas, M. G. Ramsay, N. J. Sircombe, P. Gillies, R. G. Evans, H. Schmitz, A. R. Bell, and C. P. Ridgers, Plasma Phys. Control. Fusion **57**, 1 (2015).
[43] S.-W. Bahk, P. Rousseau, T. A. Planchon, V. Chvykov, G. Kalintchenko, A. Maksimchuk, G. A. Mourou, and V. Yanovsky, Opt. Lett. **29**, 2837 (2004).
[44] S. Gordienko, A. Pukhov, O. Shorokhov, and T. Baeva, Phys. Rev. Lett. **94**, 103903 (2005).
[45] The Advanced Light Source, "Machine information," (2016).